



Cite this: *Phys. Chem. Chem. Phys.*,  
2024, 26, 20828

# Rotational spectroscopy of 2,4,6-cycloheptatriene-1-carbonitrile: facilitating the search for complex cyclic molecules in the ISM†

Gayatri Batra, <sup>ab</sup> Laura Pille,<sup>a</sup> Benjamin E. Arenas <sup>‡a</sup> and Melanie Schnell <sup>★ab</sup>

The recent astronomical observations of the simplest aromatic nitrile benzonitrile,  $c\text{-C}_6\text{H}_5\text{CN}$ , followed by a five-membered and a bicyclic CN-functionalized ring in TMC-1 have provided a significant impetus to the field for searches of cyclic complex organic molecules in space. One such example is 2,4,6-cycloheptatriene-1-carbonitrile, a seven-membered ring with a  $-\text{CN}$  group attached to the  $\text{sp}^3$ -hybridized carbon atom. With a permanent electric dipole moment of 4.3 D, this molecule is an excellent candidate for laboratory rotational spectroscopy. In this study, experiments were performed in the 2–8 GHz, 18–26 GHz, and 75–110 GHz frequency ranges in a supersonic expansion setup and a room temperature flow cell setup. The measurements across the broad frequency range of 2–110 GHz have enabled the identification and assignment of the vibronic ground state, singly substituted rare-atom isotopologues, and vibrationally excited states. Here, we report the precise determination of the rotational constants, quartic centrifugal distortion constants, nitrogen nuclear quadrupole coupling constants, as well as molecular structure in its vibronic ground state. The comprehensive rotational spectroscopy study of this molecule, covering a large frequency range, forms the basis for its future astronomical detection and thus for extending the pool of detected complex cyclic molecules.

Received 7th May 2024,  
Accepted 10th July 2024

DOI: 10.1039/d4cp01899k

rsc.li/pccp

## 1 Introduction

The advent of radio astronomy in the late 1960s has facilitated the astronomical detections of well-known as well as highly unusual molecular systems primarily *via* their rotational signatures, indicating the astonishingly rich chemical inventory present in the interstellar medium (ISM). With the state-of-the-art facilities and high-sensitivity telescopes available today, more complex molecules are becoming the target of astronomical searches.<sup>1</sup> Recent discoveries of new molecular species are not only the subject of chemical curiosity but also underline important open questions. For example, what degree of chemical complexity exists in molecular clouds, what pathways are responsible for their formation, and if there is a correlation between the highly abundant unsaturated linear chains such as polyynes and cyanopolyynes and the comparatively scarcely observed cyclic analogs.<sup>2</sup>

Among the vast array of molecular species, surpassing 300, identified in the interstellar medium or circumstellar shells,<sup>§¶</sup> the majority of these detections were made *via* their rotational spectra. For direct detection *via* its rotational signature, a molecule must possess a permanent electric dipole moment. As a result, polar molecules, despite their potentially low abundances, serve as sensitive tracers of the molecular gases present in the ISM. This prerequisite of polarity explains the existing predominance in the detection of CN-containing molecules (>15% of the total detected molecules so far),<sup>¶</sup> as they possess high values of electric dipole moments leading to intense rotational spectra which facilitate their astronomical search.

The organic chemistry on Earth is dominated by the presence of molecules containing five- and six-membered rings as building blocks of many biological compounds.<sup>3</sup> However, it was only in the year 2018 that the first cyclic aromatic molecule, the CN-functionalized benzene ring, benzonitrile,<sup>4</sup> was identified in the cold starless core TMC-1. This molecule was then subsequently detected in four other prestellar, and possibly protostellar, sources: Serpens 1A, Serpens 1B, Serpens 2, and MC27/L1521F,<sup>5</sup> suggesting a high degree of chemical

<sup>a</sup> Deutsches Elektronen-Synchrotron DESY, Notkestr. 85, 22607 Hamburg, Germany.  
E-mail: melanie.schnell@desy.de

<sup>b</sup> Institute of Physical Chemistry, Christian-Albrechts-Universität zu Kiel, Max-Eyth-Str. 1, 24118 Kiel, Germany

† Electronic supplementary information (ESI) available. See DOI: <https://doi.org/10.1039/d4cp01899k>

‡ Present address: EaStCHEM School of Chemistry, University of Edinburgh, David Brewster Road, EH9 3FJ Edinburgh, UK.

§ <https://www.astrochymist.org/>.

¶ <https://cdms.astro.uni-koeln.de/classic/molecules>.

complexity in the early star formation regions. Shortly after, evidence was found for cyano-functionalized cyclopentadiene<sup>6</sup> in TMC-1. The detection of the CN-functionalized hydrocarbons can act as a proxy for the unsubstituted molecules as most of the studied reactions of unsaturated hydrocarbons, like benzene, with a CN radical are found to be barrierless and exothermic in nature.<sup>7</sup> The detection of the five-membered and six-membered rings with CN functionalization has evoked interest in investigating the seven-membered CN functionalized ring: 2,4,6-cycloheptatriene-1-carbonitrile (hereafter, CHT-1-CN). In this work, we conducted a thorough rotational spectroscopy study of CHT-1-CN at two different rotational temperatures to facilitate its detection in the cold as well as in warmer regions of the ISM.

In warm regions of the ISM, a considerable proportion of complex molecules reside in low-lying vibrationally excited states. The transitions arising from these vibrationally excited states are commonly referred to as weeds in radio astronomy data.<sup>8</sup> These weeds can occupy many channels in a warm and dense astronomical dataset, and therefore their characterization is an important step in simplifying complex and confusion-limited spectra. Vibrationally excited states, together with isotopologues, constitute a large fraction of the many unidentified lines in the observational datasets, for example, the percentage of these unidentified lines can be as high as 70% in deep observations at Atacama Large Millimeter/submillimeter Array (ALMA) bands 3 and 6, covering 84–116 GHz and 211–275 GHz, respectively.<sup>9</sup> The assignment of vibrationally excited states and isotopologues is also important for the completeness of the astronomical catalogs, especially in the millimeter-wave region. Moreover, isotopologues are important species not only from a spectroscopic but also from a structural point of view. The assignment of singly substituted isotopologues in the rotational spectrum provides the experimentally determined rotational constants, which then lead to the construction of a comprehensive structure of the molecule in the gas phase. For CHT-1-CN, elucidating structural information is of relevance as it is a seven-membered ring with six sp<sup>2</sup>- and one sp<sup>3</sup>-hybridized carbon atoms. The structures of cycloheptatrienes and their derivatives, investigated with vibrational and rotational spectroscopic techniques, have been a subject of discussion since the early 1960s.<sup>10–13</sup> However, prior to this work, no spectroscopic data was available in the literature on CHT-1-CN.

In this manuscript, we present an extensive analysis of the rotational spectra of CHT-1-CN covering the 2–110 GHz frequency region (in parts of 2–8, 18–26, and 75–110 GHz) in two different experimental settings using the isolated, cold conditions of a supersonic expansion in the 2–26 GHz frequency range and a flow-cell experiment at elevated temperatures (~323 K) in the 75–110 GHz frequency range. The broad frequency ranges probed and the different experimental conditions employed are of significant importance here, as not only do we analyze the vibronic ground state of the molecule but we also study vibrationally excited states. In addition, the determination of the rotational constants, quartic centrifugal

distortion constants, and nuclear quadrupole coupling constants have allowed us to accurately predict the rotational transition frequencies for the ground state into the millimeter-wave region for facilitating astronomical searches.

## 2 Experimental details

The rotational spectra of CHT-1-CN were recorded over a wide frequency range spanning from 2–110 GHz. The comprehensive analysis was achieved using three chirped-pulse Fourier transform rotational spectrometers: the COMPACT spectrometer, operating within 2–18 GHz,<sup>14–16</sup> the K-band spectrometer operating within 18–26 GHz,<sup>16</sup> and the Brightspec W-band spectrometer operating within 75–110 GHz.<sup>17</sup> A detailed description of the experimentation and instruments employed here can be found in the ESI.†

The liquid sample of CHT-1-CN purchased from Sigma Aldrich (with a given chemical purity of >95%) was used without any further purification. The molecule was first measured in the range of 18–26 GHz using the K-band spectrometer, as for a molecule of this size, most intense transitions simulated with a rotational temperature of 1–3 K lie in the range of the K-band spectrometer. The measurement was extended to the low-frequency range (2–8 GHz) employing the COMPACT spectrometer to better resolve the nuclear hyperfine split transitions due to the presence of the <sup>14</sup>N nucleus. For both measurements, the sample of CHT-1-CN was loaded into a modified pulsed nozzle (a modified Parker Series 9 valve equipped with an internal heatable reservoir with an orifice diameter of 1 mm) and heated to ~311 K. With neon used as a carrier gas at 2.5 bar, the molecular vapor was supersonically expanded into the vacuum chamber. The supersonic expansion of the gas mixture into the vacuum chamber results in a rapid decrease of the rotational temperature,  $T_{\text{rot}}$ , to the range of 1–3 K. In contrast to the spectra recorded in the low-frequency region, the measurement in the high-frequency region (75–110 GHz) was performed under flow-cell conditions. The liquid sample was heated to 323 K resulting in a constant vapor pressure of 2–3 mTorr ( $2.6\text{--}4 \times 10^{-3}$  mbar) in the spectrometer chamber.

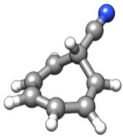
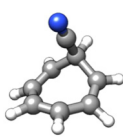
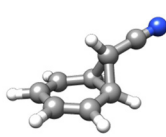
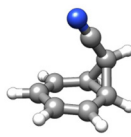
In total, 1 million FIDs in the range of 2–8 GHz, 2.2 million FIDs in the range of 18–26 GHz, and 1 million FIDs in the range of 75–110 GHz were co-added in the time domain, followed by the fast Fourier transformation into their respective frequency domains.

## 3 Theoretical details and spectroscopic analysis

To explore the conformational flexibility of CHT-1-CN, an automated semi-empirical conformational search was performed with the SPARTAN 14|| program using the Austin model 1 (AM1) method, the parameterization method 3 (PM3), and the

|| <https://www.wavefun.com>.

**Table 1** Rotational parameters, electric dipole moment components, and relative energies for the calculated lowest energy conformers and tautomers of CHT-1-CN at the B3LYP-D3/aug-cc-pVTZ level of theory

	Conformer 1	Conformer 2	Tautomer 1	Tautomer 2
				
Rotational parameters				
$A^a/\text{MHz}$	3581.7	2277.2	4304.9	2430.1
$B/\text{MHz}$	1252.7	1682.6	1161.1	1733.8
$C/\text{MHz}$	991.1	1538.8	996.7	1627.1
$\mu_a/\mu_b/\mu_c^b/\text{D}$	4.3/0.0/0.2	2.8/0.0/2.9	4.3/0.0/0.2	2.5/3.4/0.0
$\Delta E^c/\text{kJ mol}^{-1}$	0.0	6.3	22.0	24.6

<sup>a</sup>  $A$ ,  $B$ , and  $C$  are the rotational constants. <sup>b</sup>  $\mu_a/\mu_b/\mu_c$  are the electric dipole moment components. <sup>c</sup> Zero-point energy corrected relative energies.

parameterization method 6 (PM6) (Spartan 14). The results from the SPARTAN program combined with chemical intuition yielded two structures differing in the orientation of the cyano group (attached to an  $\text{sp}^3$ -hybridized carbon atom) with respect to the seven-membered ring. Moreover, the cycloheptatriene ring systems are known to undergo an equilibrium reaction between the norcaradiene–cycloheptatriene forms in the presence of electron-withdrawing groups, such as the cyano group.<sup>18</sup> Therefore, the two tautomeric forms of CHT-1-CN were also considered as a result of this equilibrium reaction. The geometry optimizations of the four structures (two conformers and two tautomers) were performed at the B3LYP-D3/aug-cc-pVTZ level of theory using the ORCA program package 5.0.<sup>19,20</sup> The computed rotational constants, dipole moment components, and zero-point corrected relative energies along with the optimized structures are summarized in Table 1.

Anharmonic frequency calculations were also performed for the lowest energy conformer to aid the analysis of the rotational spectra of the vibrationally excited states. The program package Gaussian 09<sup>21</sup> was used to perform structure optimization and anharmonic frequency calculations at the B3LYP-D3/aug-cc-pVTZ level of theory. In addition to the theoretical rotational constants corresponding to vibrationally ground and vibrationally excited states, the anharmonic frequency calculations also provided theoretical quartic centrifugal distortion constants, which are of great relevance for the assignment in the high-frequency region (75–110 GHz).

## 4 Results and discussion

CHT-1-CN is a seven-membered ring molecule containing a cyano group attached to position 1 ( $\text{sp}^3$ -hybridized C) of the ring. The structures of the two lowest-energy conformers according to the geometry optimization calculations performed at the B3LYP-D3/aug-cc-pVTZ level of theory are shown in Fig. 1. Due to the presence of an  $\text{sp}^3$ -hybridized carbon atom at position 1, the  $\pi$  electrons of the ring are not fully delocalized, giving the molecule a bent shape. Spectroscopically, CHT-1-CN is a near-oblate asymmetric top with Ray's asymmetry

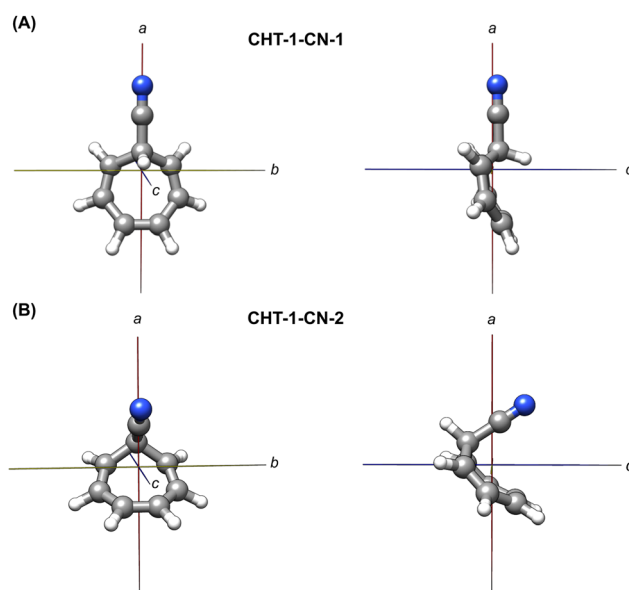


**Fig. 1** Molecular structures and principal inertia axes of the lowest energy conformers (A) CHT-1-CN-1 (top) and (B) CHT-1-CN-2 (bottom) in the  $ab$  plane (left) and in the  $ac$  plane (right).

parameter  $\kappa = \frac{2B - A - C}{A - C} = -0.79$  and  $-0.60$  for conformer 1 and 2, respectively.

### 4.1 Vibronic ground state

Among the four different structures studied computationally (Table 1), only the two lowest energy structures were observed under our experimental conditions as the rest of the structures are substantially higher in energy with respect to the lowest energy one. Hereafter, the abbreviation CHT-1-CN-1 refers to the lowest energy conformer and CHT-1-CN-2 refers to the conformer next in energy. Based on their energy difference, the Boltzmann population distribution at 323 K corresponds to 0.92 and 0.08 for CHT-1-CN-1 and CHT-1-CN-2, respectively.

As expected, the rotational spectra recorded below 26 GHz (Fig. 2) show resolvable hyperfine splitting (HFS) and the pattern of the HFS observed for the a-type transitions can be

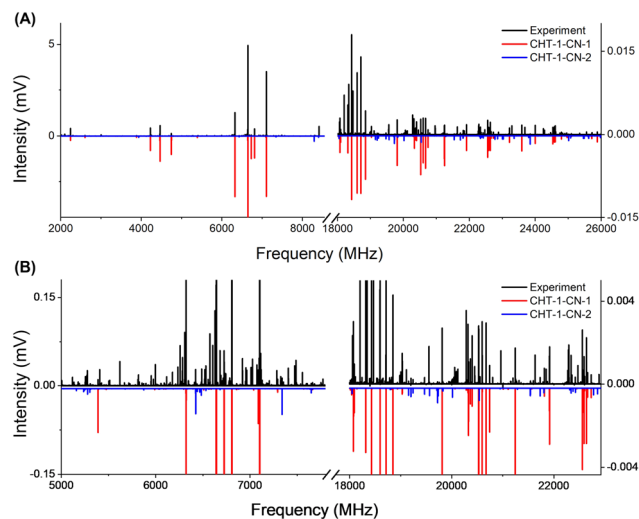


**Fig. 2** Panel (A) shows the rotational spectra of the two lowest energy conformers in the frequency range of 2–8 and 18–26 GHz. The black trace represents the experimental spectra; the red and the blue traces correspond to the simulated spectra based on the fitted rotational constants of CHT-1-CN-1 and CHT-1-CN-2, respectively, at a rotational temperature of  $T_{\text{rot}} = 3$  K. The simulated intensities are scaled with one scaling factor to match the intensities of the experimental spectra. Panel (B) shows the zoom-in to emphasize the presence of the second conformer (in blue). The left and right intensity axes correspond to the experiments performed in the different frequency regions.

found in Fig. S2 in the ESI†. The nuclear quadrupole coupling constants (NQCCs) obtained at the B3LYP-D3/aug-cc-pVTZ level of theory were used to simulate the HFS caused by the nuclear spin ( $I = 1$ ) of the  $^{14}\text{N}$  nucleus. In the present work,  $\sim 150$  and  $\sim 40$  transitions with resolved HFS were assigned for CHT-1-CN-1 and CHT-1-CN-2, respectively.

The rotational spectrum in the W-band region displayed in Fig. 3 does not show a resolvable HFS as the HFS collapses with the increasing rotational quantum number,  $J$ . For such transitions, the experimentally measured frequencies were assigned to the corresponding pure rotational transitions. For CHT-1-CN-1, the majority of the transitions were a-type transitions due to the high dipole-moment component along the  $a$ -axis. In addition to this, some c-type transitions were also assigned but no b-type transitions could be observed due to a very low dipole-moment component along the  $b$ -axis. A global fit incorporating the rotational transitions from both low- and high-frequency regions was performed. For CHT-1-CN-2, both a-type and c-type transitions were assigned in 2–26 GHz due to the significant dipole moment components along the  $a$ - and  $c$ -axes, but no transitions for CHT-1-CN-2 could be assigned in the high-frequency region. This is due to a combination of factors, such as lower overall intensities observed in the flow cell experiment at 323 K, and higher relative energy of CHT-1-CN-2 ( $\sim 6$  kJ mol $^{-1}$ ) and therefore lower abundance ( $\sim 8\%$ ) compared to the lowest energy conformer CHT-1-CN-1. In total, our data set contains 1272 assigned transitions for CHT-1-CN-1 and 123 transitions for CHT-1-CN-2 in the vibronic ground state. The experimental and theoretical rotational parameters for the

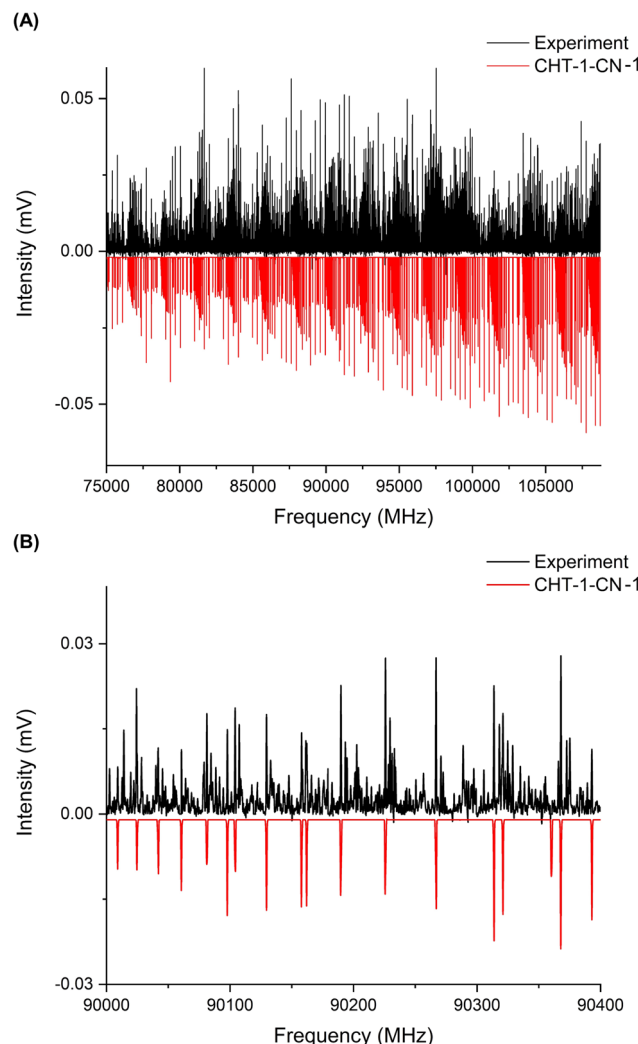


**Fig. 3** Panel (A) shows the experimental (black trace) and simulated (red trace) rotational spectrum of the vibronic ground state of CHT-1-CN-1 in the W-band region (75–110 GHz) recorded at about 323 K in a flow-cell setup. The simulated spectrum was obtained using the fitted rotational constants at a rotational temperature of  $T_{\text{rot}} \sim 323$  K. Panel (B) shows the zoom-in highlighting the well-resolved rotational transitions and also indicating the presence of rotational transitions corresponding to vibrationally excited states.

vibronic ground state of both conformers are given in Table 2, and the list of assigned transitions of both conformers can be found in Tables S3.1–S3.3 (ESI†). For CHT-1-CN-1, the line list consists of rotational transitions from 2–110 GHz, while for CHT-1-CN-2, the line list comprises of rotational transitions from 2–26 GHz. As for the case of CHT-1-CN-1, analyzing high-frequency data sets allows for the accurate determination of the centrifugal distortion constants, which are crucial for the astronomical community, as this allows one to compute reliable rest frequencies in the higher frequency region more precisely than predictions based on the rigid rotor models alone. In this work, the transition frequencies of CHT-1-CN-1 were predicted up to 150 GHz based on the fitted rotational parameters, with the use of the SPCAT program.<sup>22</sup> For the vast



**Table 2** Experimental and theoretical rotational parameters for the two lowest energy conformers, CHT-1-CN-1 and CHT-1-CN-2. The experimental rotational parameters were obtained as a result of the global fit in the frequency range 2–110 GHz and 2–26 GHz for CHT-1-CN-1 and CHT-1-CN-2, respectively. The rotational transitions were fit using Watson's A-reduction Hamiltonian in a  $I'$  representation. The theoretical rotational parameters were calculated at the B3LYP-D3/aug-cc-pVTZ level of theory

Rotational parameters	CHT-1-CN-1		CHT-1-CN-2	
	Experiment	Theory	Experiment	Theory
$A^a$ /MHz	3538.12661(62)	3581.7	2232.1100(22)	2277.2
$B$ /MHz	1251.39700(13)	1252.7	1702.8285(16)	1682.7
$C$ /MHz	990.61360(11)	991.0	1573.6604(20)	1538.8
$\Delta_f^b$ /kHz	0.055512(30)	0.053	0.683(25)	0.657
$\Delta_{JK}$ /kHz	0.20096(13)	0.196	−1.176(81)	−1.457
$\Delta_K$ /kHz	0.830(20)	0.826	0.96(11)	1.224
$\delta_J$ /kHz	0.006708(17)	0.006	0.093(17)	−0.08
$\delta_K$ /kHz	0.27771(99)	0.267	[0.145] <sup>f</sup>	0.145
$\chi_{aa}^c$ /MHz	−4.251(8)	−4.7	0.141(23)	0.09
$\chi_{bb-cc}$ /MHz	0.077(17)	0.09	4.414(38)	4.85
$\sigma^d$ /kHz	25.6		24.5	
No. of lines	1272		123	
$J/K_a^e$	54/38		5/7	

<sup>a</sup>  $A$ ,  $B$ , and  $C$  are the rotational constants. <sup>b</sup>  $\Delta_f$ ,  $\Delta_{JK}$ ,  $\Delta_K$ ,  $\delta_J$ , and  $\delta_K$  are the quartic centrifugal distortion constants. The theoretical centrifugal distortion constants were estimated from the harmonic frequency calculation with a home-written script that incorporates all the equations required for the calculation of distortion constants.<sup>24</sup> <sup>c</sup>  $\chi_{aa}$ ,  $\chi_{bb}$ , and  $\chi_{cc}$  represent the diagonal elements of the  $^{14}\text{N}$  nuclear quadrupole coupling tensor. <sup>d</sup> Microwave root-mean-square deviation of the fit. <sup>e</sup> Maximum values of  $J$  and  $K_a$  assigned in the fit. <sup>f</sup> Parameters in square brackets were kept fixed to the corresponding theoretical value.

majority of the predicted transitions, the uncertainties are well under 200 kHz. Besides the centrifugal distortion constants, the experimentally determined NQCCs,  $\chi_{aa}$  and  $\chi_{bb-cc}$ , are also important for interstellar searches, as the observation of the nuclear HFS can act as a further validation mechanism for interstellar detections. For example, the elucidation of the hyperfine splitting patterns of several interstellar molecules like cyanoallene<sup>23</sup> and benzonitrile<sup>4</sup> led to their conclusive identification in the ISM.

## 4.2 Structure determination

In the low-frequency region (2–26 GHz), in addition to the observation of the two conformers in their vibronic ground state, we also observed the rotational spectra of its singly substituted  $^{13}\text{C}$  and  $^{15}\text{N}$  isotopologues in natural abundances (1.1% and 0.4%, respectively) for CHT-1-CN-1. The presence of rotational transitions arising due to the heavy atom isotopologues can be seen through the number of unassigned lines in Fig. 2B; for the second conformer CHT-1-CN-2 in the 2–26 GHz region, the overall intensity was not sufficient to observe its singly substituted  $^{13}\text{C}$  and  $^{15}\text{N}$  isotopologues in natural abundance. In the W-band region (75–110 GHz), no rotational transitions arising from the heavy-atom isotopologues of CHT-1-CN-1 could be assigned in natural abundance. This is because, in the room-temperature measurement of CHT-1-CN, the vibrationally excited states are also populated, which increases the partition function of the molecule and

thus decreases the intensities of the respective rotational transitions.

The presence of a symmetry plane in CHT-1-CN-1 causes the effective natural abundance of the carbon atoms at equivalent positions with respect to the mirror plane, labeled as  $^{13}\text{C}(5)$ ,  $^{13}\text{C}(6)$ , and  $^{13}\text{C}(7)$  (Fig. 4, panels C and D), to be 2.2% instead of 1.1%. Since the change in the mass of the carbon atoms at equivalent positions with respect to the mirror plane has the same effect on the mass distribution, the corresponding moments of inertia and hence the rotational constants are identical. The experimentally determined rotational parameters for all the observed isotopologues of CHT-1-CN-1 (Table S4, ESI†) along with the list of all the assigned transitions arising from the singly substituted  $^{13}\text{C}$  and  $^{15}\text{N}$  isotopologues can be found in Tables S5.1–S5.6 (ESI†). These experimentally obtained rotational constants were then utilized to determine the positions of each isotopically substituted atom with respect to the molecular center of mass by employing Kraitchman's equations.<sup>25</sup> The comparison of the experimentally determined substitution structure ( $r_s$ ) and the theoretical equilibrium structure ( $r_e$ ) optimized at the B3LYP-D3/aug-cc-pVTZ level of theory is shown in Fig. 4C and D. The bold spheres represent the experimentally determined atom positions ( $r_s$ ) and the partially transparent backbone represents the equilibrium geometry ( $r_e$ ) of the molecule.

It is informative to compare the structure of CHT-1-CN-1 to the ones of related molecules like benzonitrile<sup>26</sup> and cycloheptatriene (CHT).<sup>10,27</sup> Fig. 4 depicts the ring structures of these three molecules with their relevant bond lengths and bond angles shown in Table 3. For CHT, the values were taken from gas-phase electron diffraction data since rotational spectroscopy data on the structure determination of CHT is not available in the literature. The primary distinction in the structures of benzonitrile and CHT-1-CN-1 is the degree of saturation of the bonds in the ring, and this impacts the resulting bond lengths. The structural differences between CHT and CHT-1-CN-1 arise from the substitution of a hydrogen atom with a CN group at the C(1) position. The differences in the degree of saturation between the above-mentioned systems also affect the aromaticity of the molecules. For example, benzonitrile is an aromatic molecule while CHT and CHT-1-CN-1 are non-aromatic, due to the presence of an  $\text{sp}^3$ -hybridized carbon atom at position 1. As a result, benzonitrile is a planar molecule, while CHT and CHT-1-CN-1 are bent in shape. The boat shape arrangement of CHT-1-CN-1 makes the angle at the  $\text{sp}^3$ -hybridized carbon atom C(1) the smallest ( $106.9^\circ$ ) and the bond length associated with C(1) be the longest  $r_{\text{C}(1)-\text{C}(2)} = 1.5201(20)$  Å.

## 4.3 Vibrationally excited states

The flow-cell experiment performed with the W-band spectrometer (75–110 GHz) at  $\sim 323$  K allows for the observation of not only the vibronic ground state but also the low-lying vibrationally excited states. The population in these vibrationally excited states can be calculated using the Boltzmann distribution equation, which estimates the population distribution based

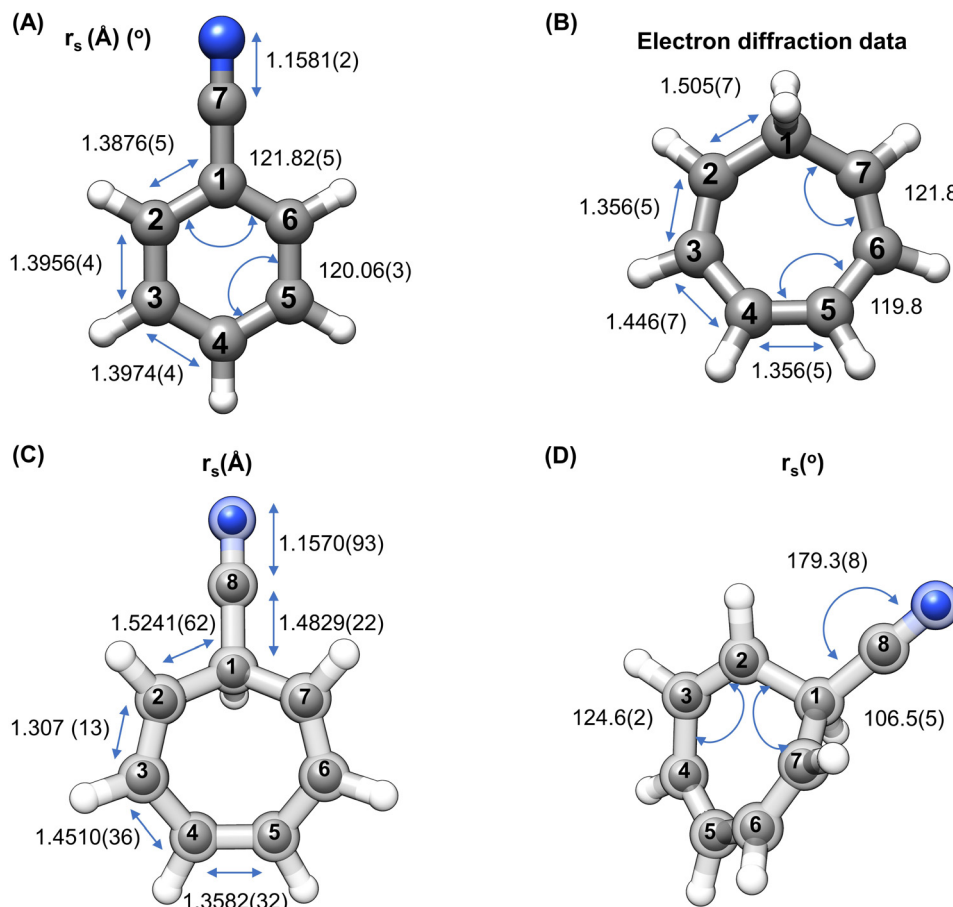


**Fig. 4** Molecular structures of (A) benzonitrile,<sup>26</sup> (B) cycloheptatriene,<sup>27</sup> (C) and (D) CHT-1-CN-1 (experimental structure determined as a part of the current study). The inner bold spheres represent the  $r_s$  positions of the atoms, whereas the partially transparent backbone gives the theoretical  $r_e$  structure (B3LYP-D3/aug-cc-pVTZ level of theory). The bond lengths are given in panel (C) and the bond angles are given in panel (D). The bond distances and angles obtained by  $r_s$  are included where available. The numbering has been arranged in a way to facilitate a more effective comparison among the three molecules.

**Table 3** Comparison of bond lengths (in Å) and bond angles (in °) between the three structurally related molecules: CHT-1-CN-1 (this work), benzonitrile,<sup>26</sup> and CHT<sup>27</sup>

CHT-1-CN-1 <sup>a</sup>		CHT <sup>b 27</sup>		Benzonitrile <sup>a 26</sup>
Bond lengths (Å)				
C(1)–C(2)	1.5241(62)	1.505(7)	C(1)–C(2)	1.3876(5)
C(2)–C(3)	1.308(13)	1.356(5)	C(2)–C(3)	1.3956(4)
C(3)–C(4)	1.4510(36)	1.446(7)	C(3)–C(4)	1.3974(4)
C(4)–C(5)	1.3582(32)	1.356(5)	C <sup>c</sup> –N	1.1581(2)
C(1)–C <sup>c</sup>	1.4829(22)			
C <sup>c</sup> –N	1.1570(93)			
Bond angles (°)				
C(1)–C(2)–C(3)	120.4(6)	121.8	C(1)–C(2)–C(3)	119.00(4)
C(2)–C(3)–C(4)	124.6(2)	127.2	C(2)–C(3)–C(4)	120.06(3)
C(3)–C(4)–C(5)	125.5(2)	119.8	C(3)–C(4)–C(5)	120.05(3)
C(2)–C(1)–C(7)	106.5(5)		C(2)–C(1)–C(6)	121.82(5)
C(1)–C <sup>c</sup> –N	179.3(8)		C(1)–C <sup>c</sup> –N	

<sup>a</sup> Parameters determined *via* the  $r_s$  method. <sup>b</sup> Parameters taken from an electron diffraction study of CHT in the gas phase. <sup>c</sup> Carbon atom of the cyano group.

on the temperature and the energy difference between the two states of interest. We present here the assignment of the six

lowest energy vibrationally excited states of CHT-1-CN-1, namely  $\nu_{42}$ ,  $\nu_{41}$ ,  $2\nu_{42}$ ,  $\nu_{42} + \nu_{41}$ ,  $\nu_{40}$ , and  $\nu_{38}$ , within 500 cm<sup>−1</sup> of energy difference relative to the ground state of CHT-1-CN-1. A brief description of the fundamental modes follows:  $\nu_{42}$  (110.4 cm<sup>−1</sup>) is an out-of-plane bending motion, this can be seen as the movement of the C–CN bond and the ring C atoms in the *ac* plane;  $\nu_{41}$  (145.7 cm<sup>−1</sup>) is an in-plane wagging motion along the C–CN bond in the *bc* plane;  $\nu_{40}$  (269.7 cm<sup>−1</sup>) is an out-of-plane wagging motion of the CN group in the *ac* plane;  $\nu_{38}$  (318.2 cm<sup>−1</sup>) is a breathing motion, shown by the periodic expansion and contraction of the ring structure.

The spectral assignment of the vibrationally excited states was facilitated by anharmonic frequency calculations performed at the B3LYP-D3/aug-cc-pVTZ level of theory, the corresponding vibrational motions are depicted in Fig. 5. The theoretical rotational constants obtained for each of the observed vibrationally excited states were shifted by the difference in the theoretical and experimental rotational constants obtained for the vibronic ground state at the same level of theory. The experimentally determined rotational constants and the number of assigned transitions for the four

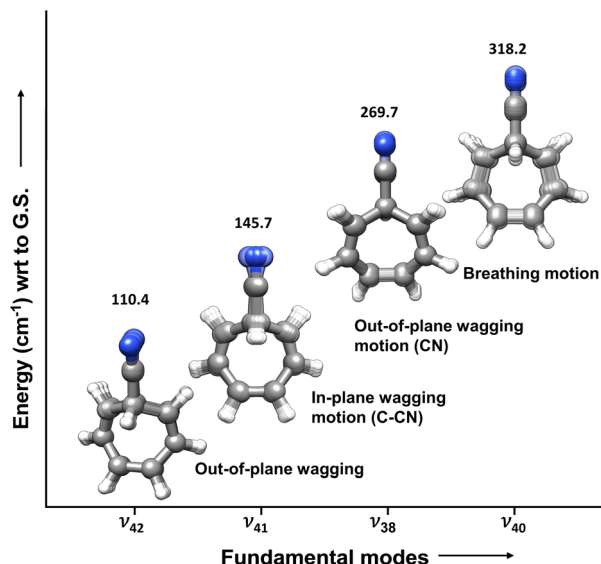


Fig. 5 A summary of the assigned fundamental vibrations of CHT-1-CN-1. The predominant motion for each mode is indicated by the overlapping transparent structures. The anharmonic energies are given with respect to the ground state and were calculated at the B3LYP-D3/aug-cc-pVTZ level of theory.

fundamental bands, as well as one overtone ( $2\nu_{42}$ ) and one combination band ( $\nu_{42} + \nu_{41}$ ), are listed in Table S6 (ESI<sup>†</sup>) along with their derived rotational constants and anharmonic energies computed at the B3LYP-D3/aug-cc-pVTZ level of theory. Table S6 (ESI<sup>†</sup>) also lists the estimated Boltzmann population calculated using the anharmonic energies of the six vibrationally excited states. The line lists of rotational transitions

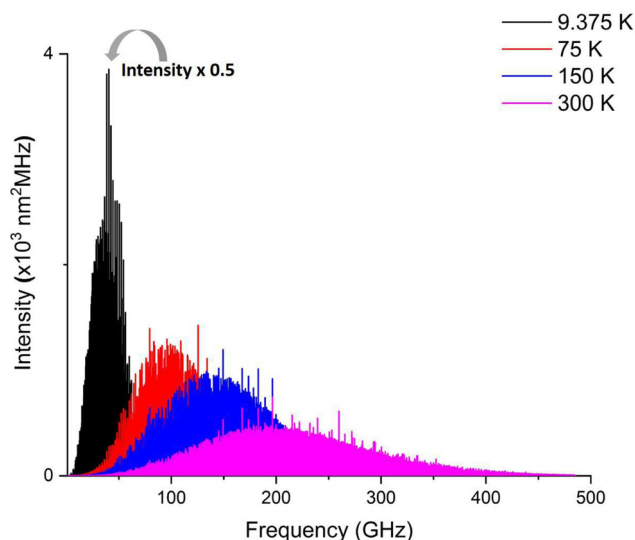


Fig. 6 Distribution of rotational transitions of CHT-1-CN-1 for four of the standard temperatures implemented in the JPL database.<sup>29</sup> The frequency simulation is made up to 500 GHz for the case of  $2I + 1 = 1$ . Note that the intensity scale for the prediction at 9.375 K has been halved for clearer comparison with the predictions at higher temperatures.

Table 4 Rotational and vibrational partition functions for CHT-1-CN-1 across the standard range of temperatures as implemented in the JPL database<sup>29</sup> and calculated using the SPCAT/SPFIT program suite<sup>30,31</sup>

$T/K$	$Q_{\text{rot}}[2I + 1 = 1]^a$	$Q_{\text{vib}}$	$Q_{\text{tot}} = Q_{\text{rot}} \times Q_{\text{vib}}$
300	717 080.21	4.41	3 162 323.74
225	565 236.67	3.31	1 870 933.38
150	374 514.46	2.14	801 460.94
75	153 657.35	1.22	187 461.96
37.5	55 464.69	1.02	56 573.99
18.75	19 624.43	1.00	19 624.43
9.375	6943.87	1.00	6943.87
1.5	448.34	1.00	448.34

<sup>a</sup>  $I = 0$  for  $^{14}\text{N}$ , ignoring the HFS.

corresponding to the vibrationally excited states are given in Tables S7.1–S7.6 (ESI<sup>†</sup>).

#### 4.4 Rotational and vibrational partition functions of CHT-1-CN-1

Interstellar searches for molecules of astronomical interest do not only require accurate rest frequencies but also information on the relative intensities of the rotational transitions. Partition functions can be used to predict the relative transition intensities at different rotational temperatures by direct summation over rotational energy levels. Further, the information on the partition functions is important for the calculation of the column densities.<sup>28</sup> The effect of temperature on the partition function is reflected in the observed transition intensities, as the increase in the temperature redistributes the population over the accessible vibrationally excited states resulting in overall lower signal intensities of the rotational transitions. A comparison of the simulated transition intensities at different temperatures for CHT-1-CN-1 is shown in Fig. 6. The plot was made considering spin degeneracy equal to 0 ( $2I + 1 = 1$ , i.e., the case where the hyperfine splitting is ignored).

The experiment in the range of 75–110 GHz was performed at  $\sim 323$  K, therefore it is important to consider the vibrational partition function in addition to the rotational partition function. In Table 4, we list the rotational ( $Q_{\text{rot}}$ ) and vibrational ( $Q_{\text{vib}}$ ) partition functions of CHT-1-CN-1 calculated for the rotational quantum number  $J$  up to 75 and up to the frequency range of 150 GHz without considering the HFS due to  $^{14}\text{N}$ . The rotational partition functions were calculated across the standard temperatures (as implemented in the jet propulsion laboratory (JPL) database<sup>29</sup>) using the SPCAT/SPFIT program suite.<sup>30,31</sup> The vibrational contributions were calculated through direct summation of all of the vibrational modes up to 500  $\text{cm}^{-1}$ . The total partition function ( $Q_{\text{tot}}$ ) of the molecule in the electronic ground state is the product of  $Q_{\text{rot}}$  and  $Q_{\text{vib}}$ , as listed in Table 4.

## 5 Conclusions

This comprehensive investigation of the rotational spectra of 2,4,6-cycloheptatriene-1-carbonitrile led to the identification and assignment of the two lowest energy conformers,

CHT-1-CN-1 and CHT-1-CN-2, in their vibronic ground states, including the assignment of the singly substituted  $^{13}\text{C}$  and  $^{15}\text{N}$  isotopologues in natural abundances. Additionally, six vibrationally excited states of CHT-1-CN-1 were also observed and characterized in the flow cell experiment at  $\sim 323\text{ K}$ .

The analysis of the vibrationally excited states is an important task, as they could act as temperature probes in regions where the ground state species is detected. Moreover, it is useful for the simplification of complex astronomical datasets by eliminating lines from vibrationally excited states and isotopologues of already known molecules.

For the lowest energy conformer CHT-1-CN-1, the assignment comprises of exact rotational frequencies in the 2–8, 18–26, and 75–110 GHz frequency ranges, leading to the determination of rotational parameters up to quartic distortion constants along with the nuclear quadrupole coupling constants. The accurate determination of centrifugal distortion constants allowed us to compute reliable rest frequencies in the high-frequency region (up to 150 GHz). For the vast majority of predicted transition frequencies, the uncertainties are well under 200 kHz, which makes this a reliable study for conducting astronomical searches. Rotational and vibrational partition functions were also calculated for the variety of temperatures as listed in the JPL database.<sup>29</sup> In addition to determining the gas-phase structure of CHT-1-CN-1 in the vibronic ground state, its structure is also compared to other similar molecules like CHT and benzonitrile. The aromatic nature of benzonitrile explains the decrease in bond lengths in the ring structure as compared to those in CHT and CHT-1-CN-1, especially the ones including the C(1) carbon atom due to its  $\text{sp}^3$  hybridization.

The astronomical detections of cyano-substituted five-membered and six-membered rings, cyanocyclopentadiene<sup>6</sup> and benzonitrile,<sup>4</sup> respectively, make this cyano-substituted seven-membered ring (CHT-1-CN-1) a potential candidate to be detected in the ISM. Moreover, the electric dipole moment of CHT-1-CN-1 (4.3 D) makes it a favorable molecule to be searched for using radio astronomy. The astronomical search for CHT-1-CN-1 is suggested in TMC-1, where other cyclic molecules have been detected recently like benzonitrile,<sup>4</sup> *o*-benzyne,<sup>32</sup> cyclopentadiene and derivatives,<sup>33,34</sup> and indene.<sup>33,35,36</sup> The comprehensive study of complex cyclic molecules like CHT-1-CN-1 opens up the possibility of investigating even more complex or cyclic molecules while testing the limits of radio astronomy.

## Author contributions

Gayatri Batra: formal analysis, validation, investigation, data curation, writing – original draft, writing – review & editing, visualization. Laura Pille: formal analysis, validation, investigation, data curation, writing – review & editing. Benjamin E. Arenas: validation, investigation, data curation, writing – review & editing, project administration. Melanie Schnell: resources, writing – review & editing, supervision, funding acquisition, and project administration.

## Data availability

The line lists of the respective species listing all the fitted rotational transitions are given in the ESI† of this manuscript. Raw data, like the overall spectra, can be obtained from the authors upon request.

## Conflicts of interest

The authors declare that they have no known competing financial interests or personal relationships that could have appeared to influence the work reported in this paper.

## Acknowledgements

The authors thank Dr Wenhao Sun and Dr Denis Tikonov for scientific discussions. We acknowledge the use of the Maxwell computational resources operated at Deutsches Elektronen-Synchrotron DESY, Hamburg, Germany.

## Notes and references

- 1 B. E. Arenas, M. Fatima, C. Pérez, S. Fischer, A. L. Steber and M. Schnell, *Astrophys. J.*, 2021, **912**, 90.
- 2 M. C. McCarthy and B. A. McGuire, *J. Phys. Chem. A*, 2021, **125**, 3231–3243.
- 3 E. Herbst and E. F. van Dishoeck, *Annu. Rev. Astron. Astrophys.*, 2009, **47**, 427–480.
- 4 B. A. McGuire, A. M. Burkhardt, S. Kalenskii, C. N. Shingledecker, A. J. Remijan, E. Herbst and M. C. McCarthy, *Science*, 2018, **359**, 202–205.
- 5 A. M. Burkhardt, R. A. Loomis, C. N. Shingledecker, K. L. K. Lee, A. J. Remijan, M. C. McCarthy and B. A. McGuire, *Nat. Astron.*, 2021, **5**, 181–187.
- 6 K. L. Kelvin Lee, P. B. Changala, R. A. Loomis, A. M. Burkhardt, C. Xue, M. A. Cordiner, S. B. Charnley, M. C. McCarthy and B. A. McGuire, *Astrophys. J. Lett.*, 2021, **910**, L2.
- 7 K. L. Kelvin Lee, B. A. McGuire and M. C. McCarthy, *Phys. Chem. Chem. Phys.*, 2019, **21**, 2946–2956.
- 8 S. M. Fortman, I. R. Medvedev, C. F. Neese and F. C. De Lucia, *Astrophys. J. Lett.*, 2010, **725**, L11.
- 9 V. Taquet, E. F. van Dishoeck, M. Swayne, D. Harsono, J. K. Jørgensen, L. Maud, N. F. W. Ligterink, H. S. P. Müller, C. Codella, K. Altwegg, A. Bieler, A. Coutens, M. N. Drozdovskaya, K. Furuya, M. V. Persson, M. L. R. van Hoff, C. Walsh and S. F. Wampfler, *Astron. Astrophys.*, 2018, **618**, A11.
- 10 C. la Lau and H. de Ruyter, *Spectrochim. Acta*, 1963, **19**, 1559–1566.
- 11 S. S. Butcher, *J. Chem. Phys.*, 1965, **42**, 1833–1836.
- 12 W. Paulick, C. Jung, U. Kempka, J. Sühnel and K. Gustav, *THEOCHEM*, 1981, **85**, 235–240.
- 13 R. A. Creswell, *J. Mol. Spectrosc.*, 1974, **51**, 111–114.
- 14 D. Schmitz, V. A. Shubert, T. Betz and M. Schnell, *J. Mol. Spectrosc.*, 2012, **280**, 77–84.
- 15 C. Pérez, A. Krin, A. L. Steber, J. C. López, Z. Kisiel and M. Schnell, *J. Phys. Chem. Lett.*, 2016, **7**, 154–160.



- 16 M. Fatima, C. Pérez, B. E. Arenas, M. Schnell and A. L. Steber, *Phys. Chem. Chem. Phys.*, 2020, **22**, 17042–17051.
- 17 B. E. Arenas, S. Gruet, A. L. Steber, B. M. Giuliano and M. Schnell, *Phys. Chem. Chem. Phys.*, 2017, **19**, 1751–1756.
- 18 L. M. Bateman, O. A. McNamara, N. R. Buckley, P. O'Leary, F. Harrington, N. Kelly, S. O'Keeffe, A. Stack, S. O'Neill, D. G. McCarthy and A. R. Maguire, *Org. Biomol. Chem.*, 2015, **13**, 11026–11038.
- 19 F. Neese, *Wiley Interdiscip. Rev.: Comput. Mol. Sci.*, 2012, **2**, 73–78.
- 20 F. Neese, *Wiley Interdiscip. Rev.: Comput. Mol. Sci.*, 2018, **8**, e1327.
- 21 M. J. Frisch, G. W. Trucks, H. B. Schlegel, G. E. Scuseria, M. A. Robb, J. R. Cheeseman, G. Scalmani, V. Barone, G. A. Petersson, H. Nakatsuji, X. Li, M. Caricato, A. V. Marenich, J. Bloino, B. G. Janesko, R. Gomperts, B. Mennucci, H. P. Hratchian, J. V. Ortiz, A. F. Izmaylov, J. L. Sonnenberg, D. Williams-Young, F. Ding, F. Lipparini, F. Egidi, J. Goings, B. Peng, A. Petrone, T. Henderson, D. Ranasinghe, V. G. Zakrzewski, J. Gao, N. Rega, G. Zheng, W. Liang, M. Hada, M. Ehara, K. Toyota, R. Fukuda, J. Hasegawa, M. Ishida, T. Nakajima, Y. Honda, O. Kitao, H. Nakai, T. Vreven, K. Throssell, J. A. Montgomery, Jr., J. E. Peralta, F. Ogliaro, M. J. Bearpark, J. J. Heyd, E. N. Brothers, K. N. Kudin, V. N. Staroverov, T. A. Keith, R. Kobayashi, J. Normand, K. Raghavachari, A. P. Rendell, J. C. Burant, S. S. Iyengar, J. Tomasi, M. Cossi, J. M. Millam, M. Klene, C. Adamo, R. Cammi, J. W. Ochterski, R. L. Martin, K. Morokuma, O. Farkas, J. B. Foresman and D. J. Fox, *Gaussian 09*, Gaussian, Inc., Wallingford CT, 2016.
- 22 Z. Kisiel, L. Pszczółkowski, I. R. Medvedev, M. Winnewisser, F. C. De Lucia and E. Herbst, *J. Mol. Spectrosc.*, 2005, **233**, 231–243.
- 23 F. J. Lovas, A. J. Remijan, J. Hollis, P. Jewell and L. E. Snyder, *Astrophys. J.*, 2006, **637**, L37.
- 24 J. K. Watson, *J. Chem. Phys.*, 1967, **46**, 1935–1949.
- 25 J. Kraitichman, *Am. J. Phys.*, 1953, **21**, 17–24.
- 26 J. Casado, L. Nygaard and G. Sørensen, *J. Mol. Struct.*, 1971, **8**, 211–224.
- 27 M. Traetteberg, *J. Am. Chem. Soc.*, 1964, **86**, 4265–4270.
- 28 J. G. Mangum and Y. L. Shirley, *Publ. Astron. Soc. Pac.*, 2015, **127**, 266–298.
- 29 H. Pickett, R. Poynter, E. Cohen, M. Delitsky, J. Pearson and H. Müller, *J. Quant. Spectrosc. Radiat. Transfer*, 1998, **60**, 883–890.
- 30 H. M. Pickett, *J. Mol. Spectrosc.*, 1991, **148**, 371–377.
- 31 Z. Kisiel, PROSPE - Programs for Rotational Spectroscopy, <http://info.ifpan.edu.pl/~kisiel/prospe.htm>, 2015.
- 32 J. Cernicharo, M. Agúndez, R. Kaiser, C. Cabezas, B. Tercero, N. Marcelino, J. Pardo and P. De Vicente, *Astron. Astrophys.*, 2021, **652**, L9.
- 33 J. Cernicharo, M. Agúndez, C. Cabezas, B. Tercero, N. Marcelino, J. R. Pardo and P. De Vicente, *Astron. Astrophys.*, 2021, **649**, L15.
- 34 J. Cernicharo, R. Fuentetaja, M. Agúndez, R. I. Kaiser, C. Cabezas, N. Marcelino, B. Tercero, J. R. Pardo and P. de Vicente, *Astron. Astrophys.*, 2022, **663**, L9.
- 35 A. M. Burkhardt, K. L. K. Lee, P. B. Changala, C. N. Shingledecker, I. R. Cooke, R. A. Loomis, H. Wei, S. B. Charnley, E. Herbst and M. C. McCarthy, *et al.*, *Astrophys. J. Lett.*, 2021, **913**, L18.
- 36 M. L. Sita, P. B. Changala, C. Xue, A. M. Burkhardt, C. N. Shingledecker, K. L. K. Lee, R. A. Loomis, E. Momjian, M. A. Siebert and D. Gupta, *et al.*, *Astrophys. J. Lett.*, 2022, **938**, L12.